



HAL
open science

Revealing the role of supernatant and granular sludge fractions on granular anaerobic membrane bioreactor fouling

Lucie Sanchez, Geoffroy Lesage, Yasar Onur Demiral, Ignasi Rodriguez-Roda, Marc Heran, Gaetan Blandin

► **To cite this version:**

Lucie Sanchez, Geoffroy Lesage, Yasar Onur Demiral, Ignasi Rodriguez-Roda, Marc Heran, et al.. Revealing the role of supernatant and granular sludge fractions on granular anaerobic membrane bioreactor fouling. *Journal of Water Process Engineering*, 2022, 49, pp.103168. 10.1016/j.jwpe.2022.103168 . hal-03808335

HAL Id: hal-03808335

<https://hal.science/hal-03808335v1>

Submitted on 10 Oct 2022

HAL is a multi-disciplinary open access archive for the deposit and dissemination of scientific research documents, whether they are published or not. The documents may come from teaching and research institutions in France or abroad, or from public or private research centers.

L'archive ouverte pluridisciplinaire **HAL**, est destinée au dépôt et à la diffusion de documents scientifiques de niveau recherche, publiés ou non, émanant des établissements d'enseignement et de recherche français ou étrangers, des laboratoires publics ou privés.

1 **Revealing the role of supernatant and granular sludge**
2 **fractions on granular anaerobic membrane bioreactor fouling**

3 Lucie Sanchez^{a,b}, Geoffroy Lesage^{a*}, Yasar Onur Demiral^{b,c}, Ignasi Rodriguez-Roda^b,
4 Marc Heran^a, Gaetan Blandin^b

5 ^a Institut Européen des Membranes (IEM), Université de Montpellier, CNRS, ENSCM,
6 Montpellier, France

7 ^b LEQUIA, Institute of the Environment, University of Girona, Spain

8 ^c Dokuz Eylül University, The Graduate School of Natural and Applied Sciences,
9 Tinaztepe Campus, Izmir, Turkey

10 *Corresponding author (e-mail: geoffroy.lesage@umontpellier.fr)

11 **ABSTRACT**

12 In order to design efficient fouling mitigation strategies in granular anaerobic membrane
13 bioreactors (G-AnMBR), foulant characteristics and their role have to be thoroughly
14 investigated. Raw mixed liquor of G-AnMBR was split by sieving into granules and
15 supernatant fractions at 0.125 mm. Then, the fouling potential and reversibility of the
16 different samples (granules, supernatant and raw mixed liquor) were assessed by
17 measuring critical fluxes and through filtration tests. Various hydrodynamic conditions,
18 i.e. gas sparging and recirculation, were applied to evaluate the impact of shear stress on
19 fouling propensity. Results revealed that the supernatant fraction, composed of fine
20 compounds and micro-particles, had a strong fouling potential, whilst the granule fraction
21 led to minor fouling filtration resistance. Three-dimensional excitation emission
22 fluorescence spectroscopy emphasised the prominent role of colloidal proteins in G-
23 AnMBR membrane fouling. During the filtration test of raw mixed liquor, the fouling

24 propensity of the micro-particles was lowered, since the structural cake layer was
25 modified. Gas sparging allowed for the mitigation of cake formation, but excess of shear
26 forces may lead to granule break-up and more irreversible fouling. Liquid recirculation
27 led to a higher filtration resistance, but almost all the membrane permeability was
28 recovered by physical cleaning. A short filtration cycle without gas sparging followed by
29 a short period of relaxation and gas sparging could be a suitable fouling mitigation
30 method. In this way, release of micro-particles from granule break-up could be limited,
31 the cake build-up would be mostly reversible by physical cleaning, and the energy
32 demand of gas sparging would be greatly reduced, thereby improving the energy
33 neutrality of the G-AnMBR biotechnology.

34 **KEYWORDS**

35 membrane; granular sludge; membrane fouling; gas sparging; membrane cleaning.

36 **1. Introduction**

37 The anaerobic membrane bioreactor (AnMBR) is an emergent biotechnology that
38 combines anaerobic digestion and membrane filtration. This hybrid technology is
39 drawing attention for domestic wastewater treatment due to its competitiveness in terms
40 of (i) conversion of organics into methane, (ii) effluent quality and (iii) reactor
41 compactness [1,2]. Many lab- and pilot-scale studies have proven that AnMBR is a
42 sustainable and efficient alternative to conventional energy-intensive processes, which
43 could be suitable for low-energy, water-scarce, low-income and space-limited areas [3,4].

44 Nonetheless, a major hindrance to AnMBR scale-up and implementation in mainstream
45 wastewater treatment is membrane fouling, as this reduces process productivity and
46 increases energy, operational and maintenance costs (e.g. chemicals, membrane
47 replacement, etc.) [1,5]. Among strategies to reduce AnMBR fouling, the granular-

48 sludge-based anaerobic membrane bioreactor (G-AnMBR) has gained prominence in the
49 last decade, since granules simultaneously boost the biomass activity and reduce
50 membrane fouling [4,6,7]. Granular sludge is characterised by a self-immobilisation of
51 biomass into compact and dense aggregates which form well-established micro-
52 ecosystems. The structural arrangement of the granules imparts high settling capacity,
53 efficient methanogenic activity and high strength to loading rates changes and shocks [2].
54 Zhang et al. (2021) found that 39.9% of fouling mitigation in a granular membrane
55 bioreactor (MBR) was due to the scouring effect of granules over the membrane surface,
56 while 50.3% was attributed to granule structure [8]. The mechanical scouring effect of
57 the granular material expanded by gas sparging has been reported effective in diminishing
58 membrane fouling in MBR by friction with the membrane and by enhancing the collision
59 between granules and suspended sludge, thus reducing their deposition [8,9]. Due to the
60 higher density of granules, granular sludge is less easily pushed towards the membrane
61 surface than suspended sludge. It is further hypothesised that the large size and solid
62 structure of granular biomass and the immobilisation of extracellular polymeric
63 substances (EPS) within granule structure limit fouling (i.e. pore blocking, deposition and
64 thickness of the cake layer on membrane surface) compared to conventional flocculated
65 sludge MBR [9,10]. Actually, Martin-Garcia et al. (2013) measured a concentration of
66 soluble microbial products (SMP) at least twice as high in a flocculated AnMBR than in
67 a G-AnMBR. Moreover, some solid and colloidal organics are adsorbed and biodegraded
68 inside the granular sludge bed, which is supposed to cause less membrane fouling [11,6].
69 [12] found that large granules ($d_p \geq 1.2$ mm) and small granules ($d_p \leq 1$ mm) were
70 associated to high flux and low membrane fouling because of loose cake layer structure
71 and less EPS-membrane adhesion, respectively. Conversely, they found that granular
72 sludge with intermediate size ($1 \leq d_p \leq 1.2$ mm) was responsible of more severe fouling

73 due to both compact cake layer and higher adhesion of EPS to membrane surface. Hence,
74 the size of granules has been also identified as a determining factor in the extent of
75 membrane fouling.

76 The granular sludge matrix is a complex mixture. Based on the size distribution, the
77 granular sludge matrix is generally divided into various fractions, such as (i) granules, (ii)
78 sludge flocs, (iii) micro-particles – including free bacteria and micro-organisms, colloidal
79 and sub-visible particles (0.45 – 15 μm), and (iv) dissolved compounds, e.g. biopolymers,
80 salts and SMP [13,14]. All these fractions could be of influent origin, the result of the
81 bacterial activity, or process dependent and they all might cause membrane fouling
82 [15,14,2]. Several studies have focused on the characterisation of the fouling phenomena
83 in conventional AnMBR. In AnMBR studies, micro-particles were found to dominate the
84 membrane fouling phenomenon [14,15]. Yao et al. (2020) suggested that cake layer
85 formation and biofouling occurred concurrently within the AnMBR, since analogous
86 organics and micro-organisms were found in micro-particle fraction and foulant
87 components. Subsequently, even though granular sludge partly helps membrane fouling
88 mitigation compared to conventional flocculated sludge, fouling concerns remain and
89 need to be better understood to define effective fouling mitigation and cleaning strategies.

90 Based on the most common MBR fouling mitigation strategy, some studies have
91 investigated different permeate fluxes (from 5 to 20 $\text{L}\cdot\text{m}^{-2}\cdot\text{h}^{-1}$ (LMH)) and specific gas
92 demand (SGD) (0.1 – 2.0 $\text{m}^3\cdot\text{m}^{-2}\cdot\text{h}^{-1}$) to identify the best operating and hydrodynamic
93 conditions for G-AnMBR to maintain high membrane permeability with low energy
94 requirements and treatment costs [16,17]. Vinardell et al. (2022) stated that operating at
95 moderate fluxes and gas sparging rates ($J_{20} = 7.8$ LMH; $\text{SGD} = 0.5$ $\text{m}^3\cdot\text{m}^{-2}\cdot\text{h}^{-1}$) could be
96 the most favourable membrane fouling control strategy in G-AnMBR and balance process
97 productivity and process economics. Wang et al. (2018a) tested continuous and

98 intermittent gas sparging regimes and filtration cycles and stated that shear rate, gas
99 sparging frequency and filtration cycle length are of high importance for delivering
100 sustained membrane filtration. Intermittent filtration associated with intermittent gas
101 sparging has been identified as the best fouling mitigation method in G-AnMBR, since
102 low residual fouling resistance and energy neutrality can be achieved [17]. However, the
103 authors suggested further investigations to properly manage operating conditions.

104 To implement suitable and affordable fouling management, it is essential to understand
105 the inherent G-AnMBR fouling phenomenon, since membrane fouling characteristics are
106 matrix-dependent. To the best of the authors' knowledge, no previous studies have
107 explicitly explored the fouling potential of an anaerobic granular sludge matrix. The aim
108 of this study is therefore to reveal the fouling potential and mechanisms of an anaerobic
109 granular sludge. To provide an in-depth assessment, the G-AnMBR mixed liquor was
110 fractionated by sieving into two parts, the granules fraction and the supernatant fraction.
111 The threshold size that distinguishes a granule from a flocculated sludge varies from 0.1
112 mm to 1 mm, depending on the study [18–20]. In this study, bioparticles above 0.125 mm
113 were regarded as granules. Filtration tests were conducted on the raw granular mixed
114 liquor, the granules fraction and the supernatant fraction to evaluate their impact on
115 membrane fouling. Since hydrodynamic conditions and the resulting shear stress are a
116 key driver in membrane fouling mitigation, two gas sparging conditions and a liquid
117 recirculation condition were tested in each filtration test. The critical flux concept and
118 resistance-in-series model were used to determine fouling rate and reversibility of each
119 fraction for the three different hydrodynamic conditions. Three-dimensional
120 excitation/emission fluorescence analyses were conducted to characterise the foulants.
121 Specific objectives are to (i) make a direct and systematic comparison of the fouling
122 behaviour of the different fractions, (ii) determine the main compounds responsible for

123 membrane fouling, (iii) find out the possible interactions between granules and
124 supernatant fractions and their effect on fouling, and (iv) identify the impact of the
125 hydrodynamic conditions on the granular sludge and fouling behaviour to increase
126 understanding and help decision making about fouling strategies.

127 **2. Materials and methods**

128 **2.1 Anaerobic granular sludge fractions**

129 Raw granular anaerobic sludge (called the “raw mixed liquor”) was taken from a
130 mesophilic (35-38°C) industrial Upflow Anaerobic Sludge Blanket (UASB) reactor
131 treating the process water from the manufacturing of recycled paper (Saica Paper
132 Champblain-Laveyron, France). Four litres of raw mixed liquor at a constant total
133 suspended solids (TSS) concentration of 10 g/L were split through a standard sieve of
134 0.125 mm mesh size. Granules retained on the sieve ($d_p \geq 0.125$) were resuspended into
135 four litres of deionised water and represent the granules fraction from now on. The four
136 litres of liquid and particles that flowed through the sieve were regarded as the supernatant
137 fraction ($d_p < 0.125$). Fouling propensities of (i) granules, (ii) supernatant, and (iii) raw
138 mixed liquor were systematically assessed.

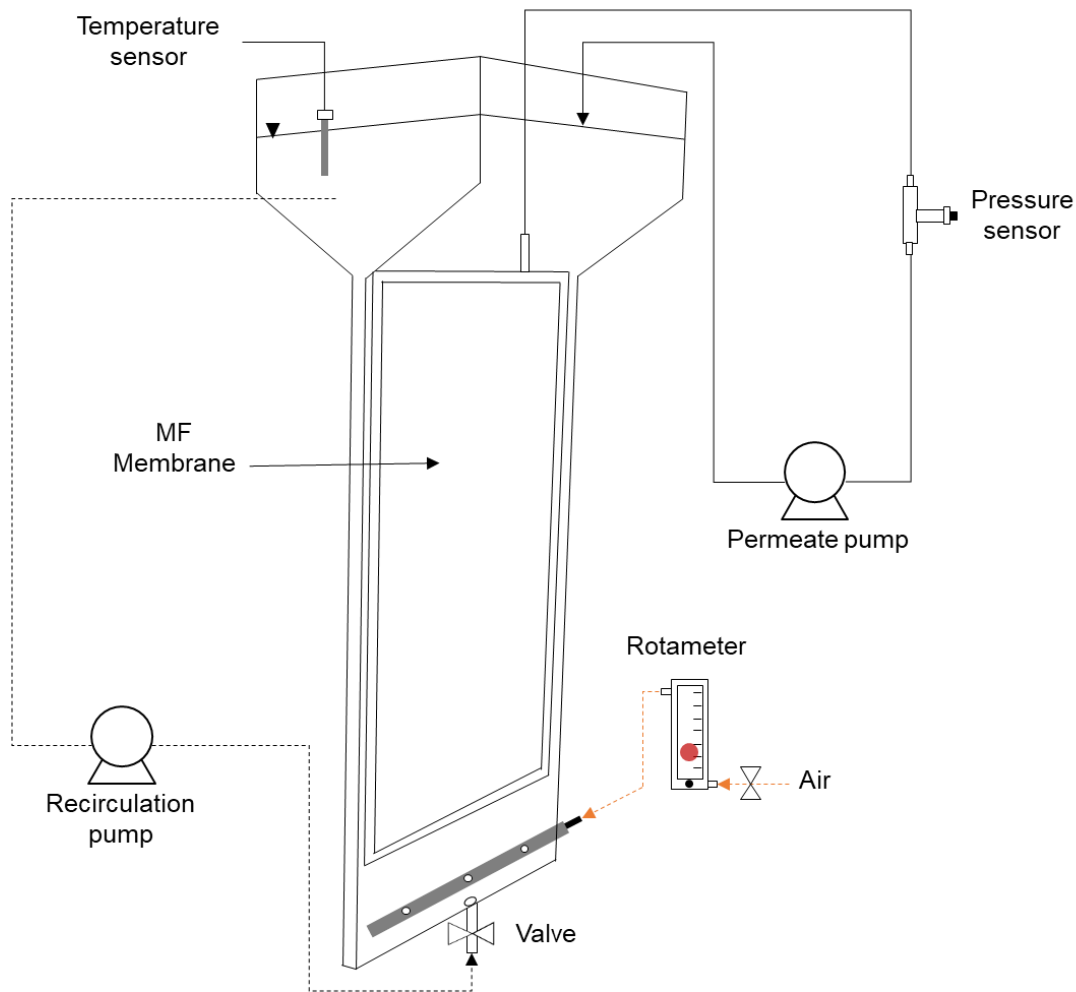
139 **2.2 Experimental set-up**

140 The experimental lab-scale system, shown in Fig. 1, was composed of two sections with
141 an effective volume of 4 L. The lower part of the reactor consisted of a thin parallelepiped-
142 shaped zone (215 x 24 x 405 mm) where the membrane cartridge was immersed and the
143 upper part was a flared section. The bottom of the reactor included both a liquid
144 recirculation and an aeration diffuser used separately according to the operating
145 conditions applied. The liquid recirculation was carried out by a peristaltic pump (Watson
146 Marlow (WMFTG), UK). Supernatant was pumped from the top of the reactor and

147 reintroduced under the membrane through a 10 mm hole placed in the middle of the
148 section. The gas sparging was done by a hollow tube with three drilled holes (1 mm
149 diameter) distributed along the length and controlled by a gas flowmeter. The
150 microfiltration membrane used was a flat sheet module from KUBOTA Membrane
151 Europe (UK) in Polyethylene Terephthalate (PET) and Chlorinated Polyethylene (PE-C)
152 with a nominal pore size of 0.4 μm , 0.11 m^2 surface area and 6 mm cartridge width. The
153 permeate was suctioned through a peristaltic pump (Watson Marlow (WMFTG), UK) and
154 returned to the reactor to maintain a constant volume. The transmembrane pressure (TMP)
155 was obtained through a pressure gauge installed on the permeate line. The water
156 temperature (T) in the reactor was monitored. Pressure and temperature data were
157 recorded using a Bluetooth-based system provided by Instrument Works (Waterloo,
158 Australia). Visualisation, acquisition and storage of all data was realised thanks to the
159 Dataworks software (Instrument Works, Waterloo, Australia). Membrane flux (J_T) was
160 set at 20 $\text{L}\cdot\text{m}^{-2}\cdot\text{h}^{-1}$ (LMH) and the corresponding normalised flux at 20°C (J_{20}) was
161 recalculated using Equation (1).

$$J_{20} = \frac{J_T \cdot \mu_T}{\mu_{20}} \quad (1)$$

162 where J_{20} is the normalised flux at 20°C ($\text{m}^3\cdot\text{m}^{-2}\cdot\text{s}^{-1}$) and μ_{20} and μ_T (in Pa.s) are the
163 viscosity of water at 20°C and at the working temperature T (°C) respectively.



164

165 Fig. 1 – Schematic representation of the experimental set-up

166

167 2.3 Filtration tests

168 Filtrations tests were conducted for the three sludge fractions (raw mixed liquor, granules
 169 and supernatant). Each experiment consisted of filtration tests based on five consecutive
 170 operating cycles composed of 45 min of filtration and 90 s of relaxation. Three
 171 hydrodynamic conditions were investigated with the aim of evaluating the influence of
 172 turbulence on filtration performances. Hence, a liquid recirculation of 24 L/h (RE) and
 173 two aeration flow rates of 25 L/h (A25) and 100 L/h (A100) were applied resulting in
 174 shear stress of 15, 205 and 409 s⁻¹ respectively (see equations in supplementary data). For
 175 RE, the crossflow velocity was about 11 m/h and the specific gas demand was 0.23 and

176 0.91 m³.m⁻².h⁻¹ for A25 and A100, respectively. Before each filtration test, the
 177 permeability of the clean membrane was measured with deionised water through flux-
 178 stepping increments and determined as follows:

$$J_{20} = Lp \cdot TMP \quad (2)$$

179 where Lp is the permeability (L.m⁻².h⁻¹.bar⁻¹), J_{20} is the normalised flux at 20°C (L.m⁻².h⁻¹)
 180 and TMP is the transmembrane pressure (bar).

181 2.4 Critical flux

182 Critical fluxes (J_c), corresponding to the onset of prominent fouling, were assessed by the
 183 flux-step method [21] for each fraction and hydrodynamic condition tested. The
 184 permeation rate was increased stepwise from 2 LMH to 30 LMH and then incrementally
 185 decreased. The corresponding TMP was continually recorded. The step duration was
 186 fixed at 10 minutes and a step height of 2 LMH and 4 LMH was chosen for the ascending
 187 and descending phases, respectively. Le Clech et al. (2003) established three key TMP -
 188 based parameters to determine the critical flux, namely: (i) the initial TMP increase (ΔP_n),
 189 (ii) the TMP increase rate $(dTMP/dt)_n$, and (iii) the average TMP ($P_{average}$)_n. All these
 190 parameters are depicted below:

$$\Delta P_n = TMP_i^n - TMP_f^{n-1} \quad (3)$$

$$(dTMP/dt)_n = \frac{(TMP_f^n - TMP_i^n)}{t_f^n - t_i^n} \quad (4)$$

$$P_{average_n} = \frac{TMP_i^n + TMP_f^n}{2} \quad (5)$$

191 where TMP_i^n and TMP_f^n are the initial and final TMP , respectively, of the n flux step, t_i^n
 192 is the starting time and t_f^n is the ending time of this step.

193 The three parameters were calculated for each flux step. When the TMP-based parameters
194 were no longer constant between flux steps and deviated from clean water values, the
195 critical flux was considered to have been reached. The critical flux values given in this
196 study are the average of the critical flux obtained through each parameter. Hence, the
197 critical flux mentioned in this study is not in its zero-rate strict form, but corresponds to
198 the flux level under which a sustainable filtration can be achieved.

199 **2.5 Fouling propensity and fouling reversibility**

200 Filtration resistances were determined following Darcy's law (Equation (6)).

$$R_t = \frac{TMP}{\mu_{20} \cdot J_{20}} \quad (6)$$

201 where R_t is the resistance (m^{-1}) and TMP is the transmembrane pressure (Pa).

202 Membrane fouling was characterised by means of the resistance-in-series model. In this
203 study, the total resistance (R_t) is defined as the sum of the intrinsic membrane resistance
204 (R_m) and the fouling resistance (R_f) which, in turn, was divided into the resistances caused
205 by reversible fouling, irreversible fouling and residual fouling ($R_{reversible}$, $R_{irreversible}$,
206 $R_{residual}$ respectively) as described in Equation (7) and (8).

$$R_t = R_m + R_f \quad (7)$$

$$R_f = R_{reversible} + R_{irreversible} + R_{residual} \quad (8)$$

207 The above-mentioned resistances were determined by filtering deionised water in the
208 same hydrodynamic conditions as the filtration tests, using the following experimental
209 procedure: (i) R_m was measured by filtering deionised water through the clean membrane;
210 (ii) R_t was evaluated using the fouled membrane at the end of the filtration test; (iii) R_f
211 was deduced from Equation (7); (iv) superficial cleaning with water was undertaken,
212 taking the fouled membrane out of the reactor and flushing the surface with 1 litre of
213 deionised water, after which the remaining resistances ($R_{irreversible} + R_{residual}$) were

214 measured by filtering deionised water; $R_{\text{reversible}}$ was then calculated using Equation (8);
215 finally, (v) a two-hour chemical cleaning by soaking in a 0.2% sodium hypochlorite
216 solution was carried out under aeration, and the leftover resistance R_{residual} was measured;
217 $R_{\text{irreversible}}$ was then deducted from Equation (8).

218 **2.6 Analytical methods**

219 **2.6.1 Particle size distribution**

220 Particle size distribution (PSD) was performed on the raw mixed liquor before and after
221 filtration tests at A25, A100 and RE. Size fractionation was done by wet sieving. The
222 standard sieves used were of 1.0, 0.63 and 0.125 mm mesh sizes, resulting in four
223 fractions: large granules ($d_p \geq 1$), medium granules ($d_p 1-0.63$), small granules ($d_p 0.63-0.125$),
224 and flocs and fines ($d_p < 0.125$). Total solids of each fraction were measured according to
225 Standard methods [22]. The PSD was expressed as a fraction's mass distribution [2].

226 **2.6.2 Three-dimensional excitation emission matrix fluorescence**

227 Three-dimensional Excitation Emission Matrix (3DEEM) fluorescence was used to
228 characterise and semi-quantify the dissolved and colloidal organic matter (DCOM), as
229 3DEEM samples were filtered at 0.45 μm . The cleaning water from the physical cleaning
230 and the raw mixed liquor before and after filtration tests were analysed. Three-
231 dimensional excitation emission matrices were obtained using a Perkin-Elmer FL6500
232 spectrometer (USA). Excitation and emission scan ranges were fixed at 200-500 nm and
233 280-600 nm, respectively, while scan speed was set at 12,000 nm/min, incremented to 10
234 nm. The slit width was 5 nm for both excitation and emission. Every sample was
235 associated with a Milli-Q water blank analysed in the same conditions. To circumvent the
236 over-quantification caused by Raman and Rayleigh water scatter peaks, all spectra were
237 scatter-corrected by the blank sample [23]. From the 3DEEM spectra, four regions were
238 distinguished, based on their specific fluorophores [24]. Region I+II was associated with

239 protein-like fluorophores (tyrosine) ranging from $\lambda_{\text{ex}} = 200\text{-}250\text{nm}$ to $\lambda_{\text{em}} = 280\text{-}380\text{nm}$,
240 Region III ($\lambda_{\text{ex}} = 200\text{-}250\text{nm} / \lambda_{\text{em}} = 380\text{-}600\text{nm}$) corresponded to fulvic acid-like
241 molecules, Region IV ($\lambda_{\text{ex}} = 250\text{-}350\text{nm} / \lambda_{\text{em}} = 280\text{-}380\text{nm}$) was associated with soluble
242 microbial product (SMP)-like molecules (Tryptophan), and Region V ($\lambda_{\text{ex}} = 250\text{-}$
243 $500\text{nm} / \lambda_{\text{em}} = 380\text{-}600\text{nm}$) corresponded to humic acid-like molecules. Region III and
244 IV were merged into a single region III+IV, called humic substances. The normalised
245 volume of fluorescence (in arbitrary unit per nm^2 (A.U./ nm^2)) beneath each area was
246 calculated as a function of the fluorescence intensity at each excitation-emission pair.

247 **2.6.3 Proteins and polysaccharides**

248 Protein (PN) and polysaccharide (PS) contents were used to characterise the different
249 fractions and to follow any modification or release of these organic compounds during
250 the experiments. The colorimetric Lowry and Dubois methods were used for PN and PS,
251 respectively [25,26]. Bovine Serum Albumin (BSA) and glucose were used as calibration
252 solutions. All samples were pre-filtered through a $0.45\ \mu\text{m}$ acetate cellulose filter before
253 dosing.

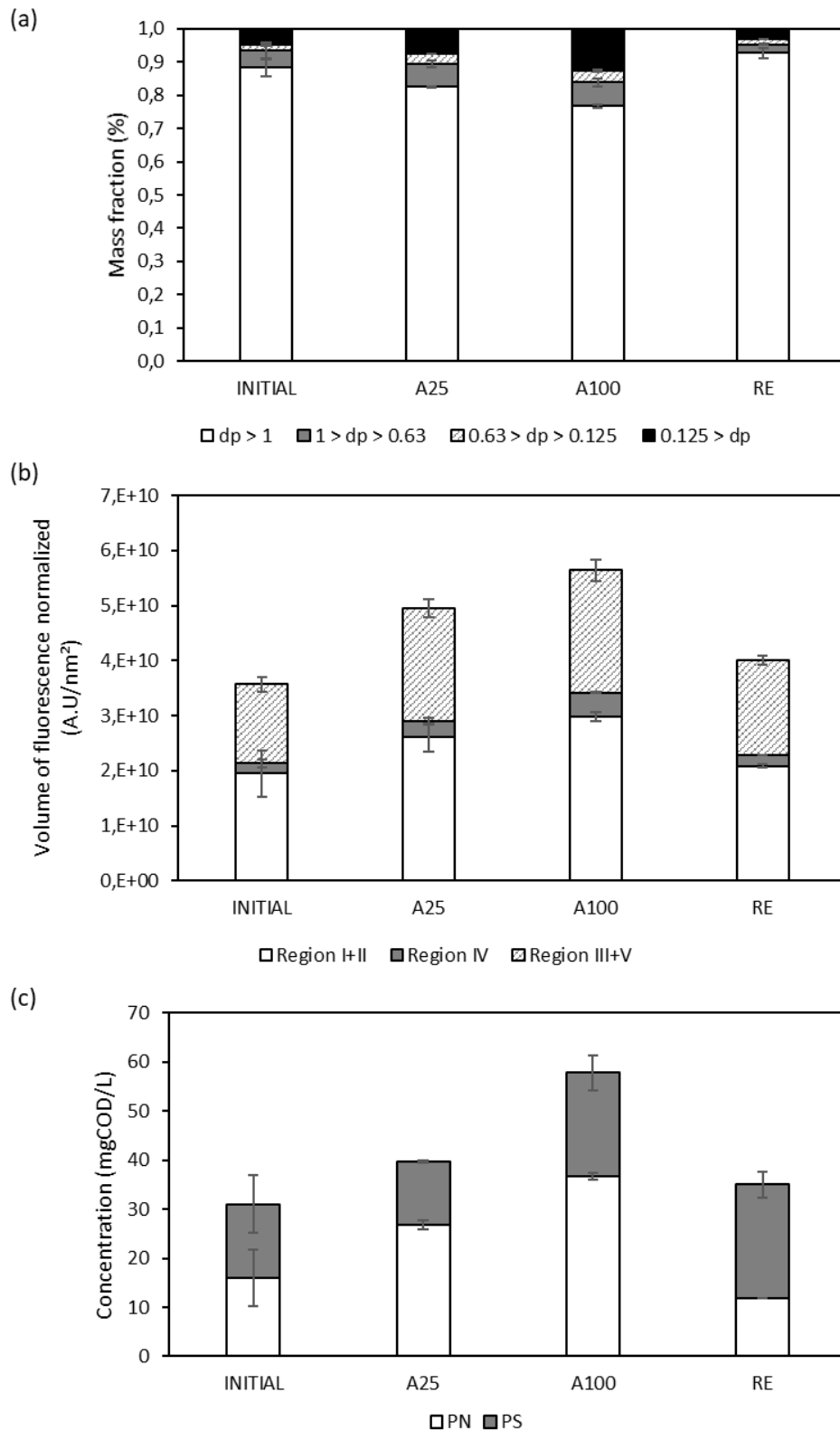
254 **3. Results and discussion**

255 **3.1 Granular sludge characteristics' behaviour during the filtration test**

256 In order to follow the raw mixed liquor trends during the filtration test, particle size
257 distribution (Fig. 2a), total volume of fluorescence (Fig. 2b), and PS and PN
258 concentrations (Fig. 2c) were measured. The initial raw mixed liquor was mainly
259 composed of large granules, i.e. around 95% of mass fraction of particles over $0.125\ \text{mm}$
260 in diameter ($d_p \geq 0.125$). Initially, the DCOM of the raw mixed liquor was predominantly
261 composed of proteins ($54.2 \pm 4.0\%$) and humic substances ($40.9 \pm 5.0\%$) and with a total
262 volume of fluorescence of $3.6 \pm 0.5 \cdot 10^{10}$ A.U. $\cdot\text{nm}^2$. The recirculation (RE) condition had

263 a slight effect on the PSD with a lower proportion of smaller compounds, probably due
264 to the aggregation of particles resulting from the low shear rate, however, no significant
265 change in organic composition was observed. In contrast, in the A25 and A100
266 conditions, the large granule content ($d_p \geq 1.0$) decreased from 88% to 83% and 77%,
267 respectively, showing that higher shear stress increased the number of smaller granules.
268 In the same way, the volume of fluorescence reached $4.9 \pm 0.5 \cdot 10^{10}$ and $5.6 \pm 0.3 \cdot 10^{10}$
269 A.U./nm² for A25 and A100, respectively, that is, +40% and +58% more than the initial
270 value. Similarly, the concentration of PN increased especially for both aeration rates A25
271 and A100 (+67% and +129%, respectively) confirming the release of protein substrates
272 from the granules. The greater the forces of attrition, the higher the total volume of
273 fluorescence and proteins became, underlining granule degradation and its release of fines
274 and DCOM. This confirmed the pre-established positive correlation between
275 hydrodynamic forces, attrition forces and granule disruption. Granule attrition created
276 crevices on the granule surface and pushed surface bacteria and DCOM off the granule
277 [27]. Moreover, soluble COD (sCOD) membrane removals are shown in supplementary
278 materials. The sCOD removal rate was globally not affected by the hydrodynamic
279 conditions, as the sCOD rejection was constant and about 27.2 ± 10.5 %.

280



281

282 Fig. 2 - Evolution of (a) Particle Size Distribution (PSD), (b) relative percentage volume of fluorescence
 283 from 3DEEM and (c) concentration of PN and PS of the raw mixed liquor before the experiment (initial)
 284 and after each hydrodynamic operating condition applied (A25, A100, RE).

285

286

3.2 Effect of sludge fraction and operating conditions on critical flux

287

The critical flux results are given in Fig. 3. In all conditions, the granule fraction showed

288

lower fouling potential, with the lowest TMP in all conditions applied, which resulted in

289

highest critical flux values ($J_c > 22$ LMH) (Fig. 3d). The TMP profiles also showed that

290

no incremental effect occurred when the supernatant and granules were both present in

291

the raw mixed liquor. Hence, the supernatant was found to be the major foulant,

292

emphasised by the lower and similar critical fluxes of both the raw mixed liquor and

293

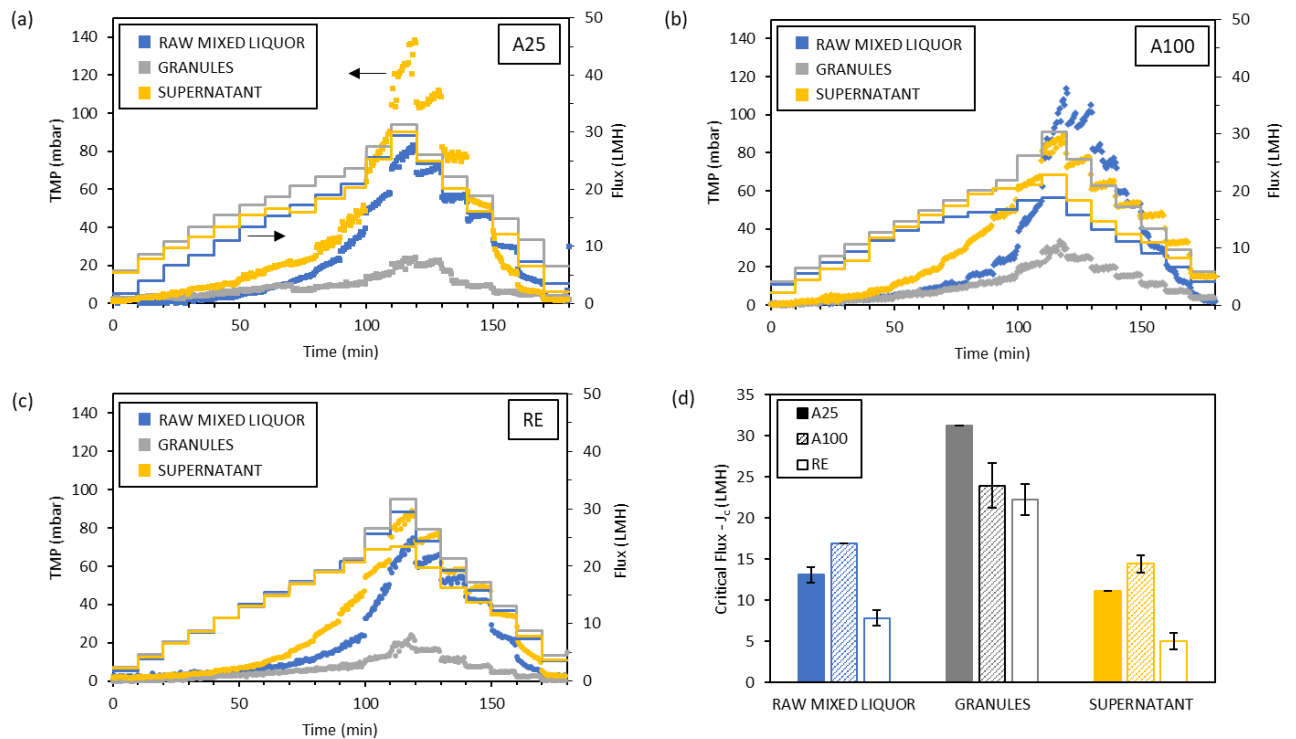
supernatant fractions. These results support those observed in recent studies which stated

294

that micro-particles ($0.45\text{-}10\mu\text{m}$) – including some colloids – were mainly responsible for

295

membrane fouling in AnMBR [13,14,28].



296

297

Fig. 3 – Evolution of TMP and flux for the raw mixed liquor and the two fractions at the different operating

298

conditions (a) A25, (b) A100, (c) RE and the (d) critical flux obtained through the TMP-based indicators.

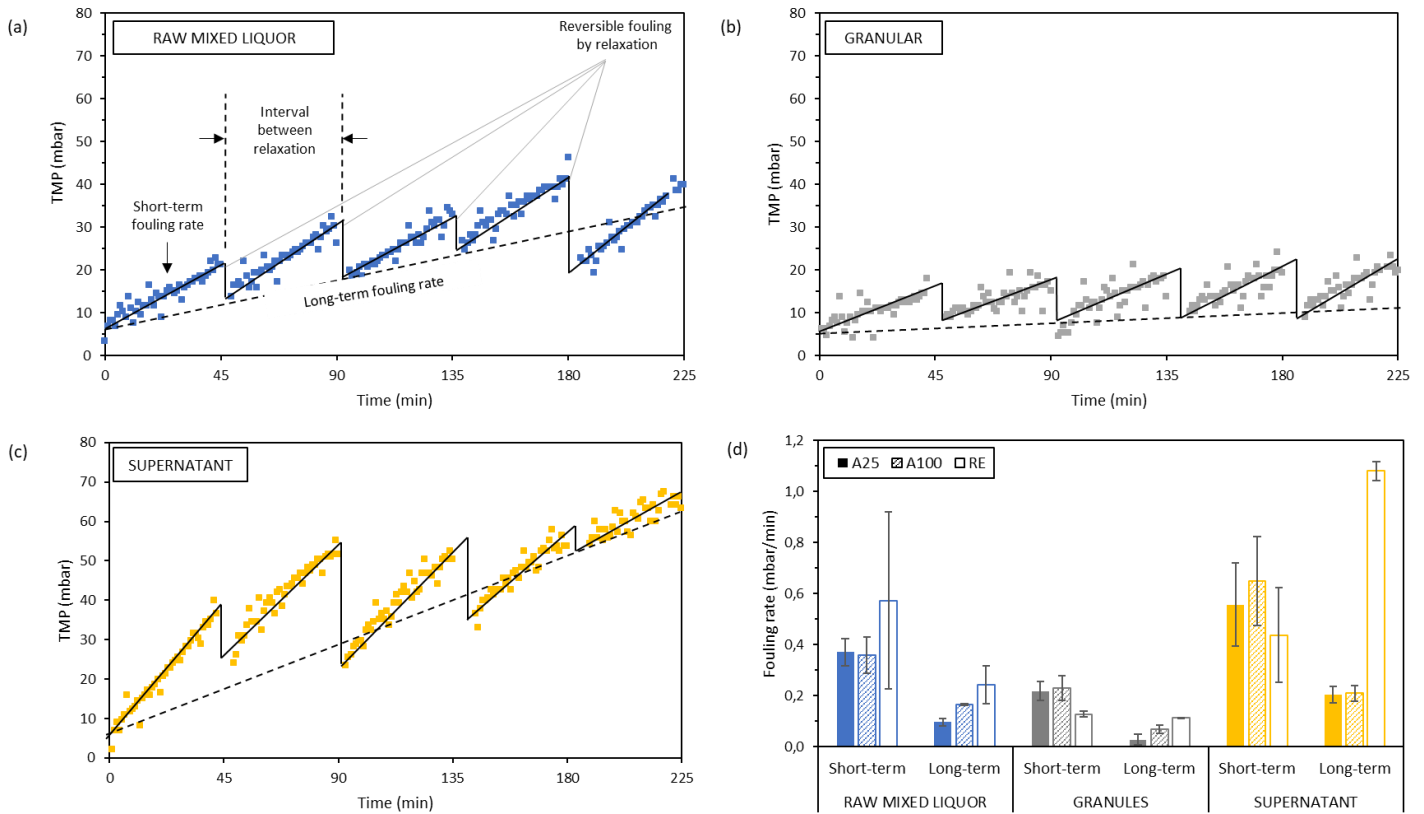
299

300 The increase in hydrodynamic conditions, induced by gas sparging, had a beneficial effect
301 on filtration performance, since the critical flux values were positively related to the shear
302 stress, except for the granule fraction (Fig. 3d). In the latter case, hydrodynamic
303 conditions were too high and detrimental for the granule filtration capacity with a drop in
304 critical flux from 31.3 LMH in A25 condition to 24 LMH for A100. This phenomenon
305 can be linked to the granule disruption mentioned earlier which led to a rise of fine
306 particles and colloidal and dissolved compounds (Fig. 2). These findings support that
307 shear forces are of high importance in mitigating membrane fouling but the use of gas
308 scouring as a fouling mitigation method has to be precisely adapted to avoid the
309 detrimental effect of the shear stress, such as granular biomass disruption, membrane
310 fouling by fines, and energy overspending.

311 In addition, while comparing the TMP reached during the flux increasing phase and
312 decreasing phase, several phenomena were observed. An apparent hysteresis was
313 observed, for the supernatant fraction and raw mixed liquor especially, suggesting non-
314 reversible fouling by the tested turbulence (see supplementary data). Interestingly, below
315 the critical flux, the gap between the ascending TMP and the descending TMP was
316 reduced in conditions A25 and A100. This phenomenon highlights that above the critical
317 flux, there was still an accumulation of foulant on the membrane surface. Conversely,
318 below the critical flux, no significant deposition of particles occurred, so during the
319 decreasing phase, the TMP declined because of the flux reduction and the cake layer
320 detachment under the aeration effects. Nevertheless, the granule fractions showed no
321 apparent hysteresis under both aeration conditions, meaning that particle deposition was
322 mostly reversible regardless of flux. Finally, in the RE condition, a strong level of
323 hysteresis was observed for all fractions. During the decreasing flux steps, the TMP

324 dropped linearly, which emphasised the absence of additional accumulation and a lack of
 325 foulant detachment [29].

326 **3.3 Membrane filtration behaviour**



327

328 Fig. 4 – Evolution of the TMP over time during the five cycles of filtration with aeration at 25L/min for
 329 (a) the raw mixed liquor, (b) granules, (c) supernatant and (d) the corresponding average reversible fouling
 330 rate for each filtration condition (A25, A100, RE) and for raw mixed liquor and the two fractions.

331

332 The change in TMP during the filtration tests of raw mixed liquor and the two fractions
 333 for the A25 condition are presented in Fig. 4. An overview of the A100 and RE conditions
 334 is provided in the supplementary data. From these TMP profiles, two fouling rates were
 335 determined: (i) the average short-term fouling rate, which corresponds to the mean fouling
 336 rate observed between intermittent relaxation steps and (ii) the long-term fouling rate
 337 (Fig. 4a and Fig. 4d). First, the lowest fouling capacities of the granule fraction were
 338 confirmed, whatever the hydrodynamic conditions, with a negligible TMP increment

339 (~0.1-0.2 mbar.min⁻¹) during operation cycles. In comparison, the supernatant presented
340 a TMP increase almost three times higher (~0.45-0.65 mbar.min⁻¹), highlighting its
341 stronger fouling propensity. This is in accordance with previous results which stated that
342 the membrane permeability declines with the decrease of the particle size deposition
343 which forms a more compact fouling deposit and leads to higher pore blocking [8,30].
344 Interestingly, under aeration conditions (A25 and A100), the raw mixed liquor sample,
345 which combines granules and supernatant fractions, exhibited TMP profiles and fouling
346 rates below the supernatant ones, with a short-term fouling rate around 0.35 mbar.min⁻¹,
347 confirming the benefit effect of granules upon the supernatant fouling behaviour. Indeed,
348 it has been reported that the granular sludge structure is largely favourable for membrane
349 mitigation due to the larger particle diameter than membrane pore, leading to low pore
350 blocking. Moreover, when combined with gas sparging, the granules had an additional
351 scouring effect, which helped to diminish the flocs accumulation on the membrane
352 surface and decrease the penetration driving force of fine particles on membrane pores
353 [8].

354 With regards to the hydrodynamic conditions applied, no significant differences were
355 observed for short-term fouling rates between the A25 and A100 conditions, regardless
356 of the fraction filtered. Numerous studies have shown that there is a critical gas velocity
357 above which the gas sparging flow rate no longer impacts the fouling rate [11,17,31].
358 Above the threshold gas sparging rate, the increase of shear stresses has no additional
359 effect on particle deposition mitigation and the coalescence of the air bubbles can even
360 reduce the shear events in the vicinity of the membrane [32]. Furthermore, the back-
361 transport resulting from the hydrodynamic conditions has been positively correlated to
362 the particle size, meaning that smaller particles face lower shear-induced diffusion

363 [33,34]. Hence, it is likely that membrane fouling in G-AnMBR is mainly a result of
364 smaller compounds and dissolved matter.

365 Moreover, the long-term fouling rate values (Fig. 4d) for the A100 condition were found
366 to be higher than the A25 for the granules and raw mixed liquor (0.07 vs 0.03 mbar.min⁻¹
367 and 0.16 vs 0.10 mbar.min⁻¹ respectively). This phenomenon is almost certainly due to
368 the attrition of the granules that increased the amount of smaller compounds (see Fig. 2a),
369 as well as extracellular polymeric substances [31], which might contribute to membrane
370 fouling that is less responsive to the relaxation step. Moreover, for the granule fraction
371 with RE condition, the short-term and long-term fouling rates were almost similar,
372 suggesting that the relaxation steps did not have a significant fouling mitigation effect.
373 Conversely, the RE condition is the least effective solution for fouling management when
374 fine compounds ($d_p < 0.125$) are in abundance (i.e. raw and supernatant samples), probably
375 due to a lack of shear events at the water-membrane interface. These filtration tests
376 support the careful consideration that should be given to the hydrodynamic parameters in
377 G-AnMBR. Shear conditions have to be great enough to prevent membrane fouling and
378 provide a long-lasting filtration, but not too high to avoid excessive energy consumption
379 and adverse effects on granular biomass. This is of great importance, because the damage
380 of granular sludge does not only have a detrimental effect on membrane fouling, but it
381 also reduces the organic removal efficiency, since biomass activity and syntrophic
382 associations are hindered [4,35].

383 **3.4 Filtration resistance**

384 Fig. 5 shows the filtration resistances measured at the successive stages of the filtration
385 tests and the different types of fouling deducted from the resistance-in-series. A
386 significant difference was observed between the resistance recorded at the end of the
387 filtration test and the total resistance measured on the fouled membrane by filtering

388 deionised water, notably for the A25 and A100 conditions. Therefore, the average total
389 resistances measured during the 10 last minutes of fifth filtration cycle are also presented
390 in Fig. 5. This difference may be due to the concentration polarisation occurring during
391 the filtration of fractions but mainly to the manipulation of the membrane and aeration
392 shear stresses during the permeability measurement, which unintentionally contributed to
393 removing the fouling during the total resistance measurement. In fact, it is as if a
394 membrane cleaning by gas sparging had been performed. Nonetheless, these facts show
395 that the filtration resistances caused by cake build-up were easily suppressed by gas
396 sparging and, therefore, counted as reversible fouling.

397 The higher fouling potential of the supernatant fraction and the synergetic effect between
398 granules and supernatant fractions were confirmed by the total resistance, measured at
399 the end of the fifth filtration cycle, which diminished from $14.2 \cdot 10^{11} \text{ m}^{-1}$ for supernatant
400 filtration to $7.5 \cdot 10^{11} \text{ m}^{-1}$ for raw mixed liquor in A25 condition, from $13.6 \cdot 10^{11}$ to $8.5 \cdot 10^{11}$
401 m^{-1} at A100, and from $60.7 \cdot 10^{11}$ to $33.3 \cdot 10^{11} \text{ m}^{-1}$ at RE. In the presence of granular sludge,
402 it has been reported that the cake layer built on the membrane surface had a lower
403 filtration resistance by means of a high cake porosity and the collision of granules with
404 flocs, biopolymers and membrane surface (Zhang et al., 2020; Zhang et al., 2021). These
405 results clearly show that the lack of shear stress in the vicinity of the membrane (e.g. RE
406 condition) led to a stronger increase in fouling resistance, since the applied shear forces
407 were not sufficient to counteract the penetration driving forces [8] and to promote the
408 scouring effect of the granules. It should be noticed that in the RE condition, constant
409 filtration fluxes were difficult to sustain and thus high resistance variabilities were
410 observed in the experiment (see supplementary material).

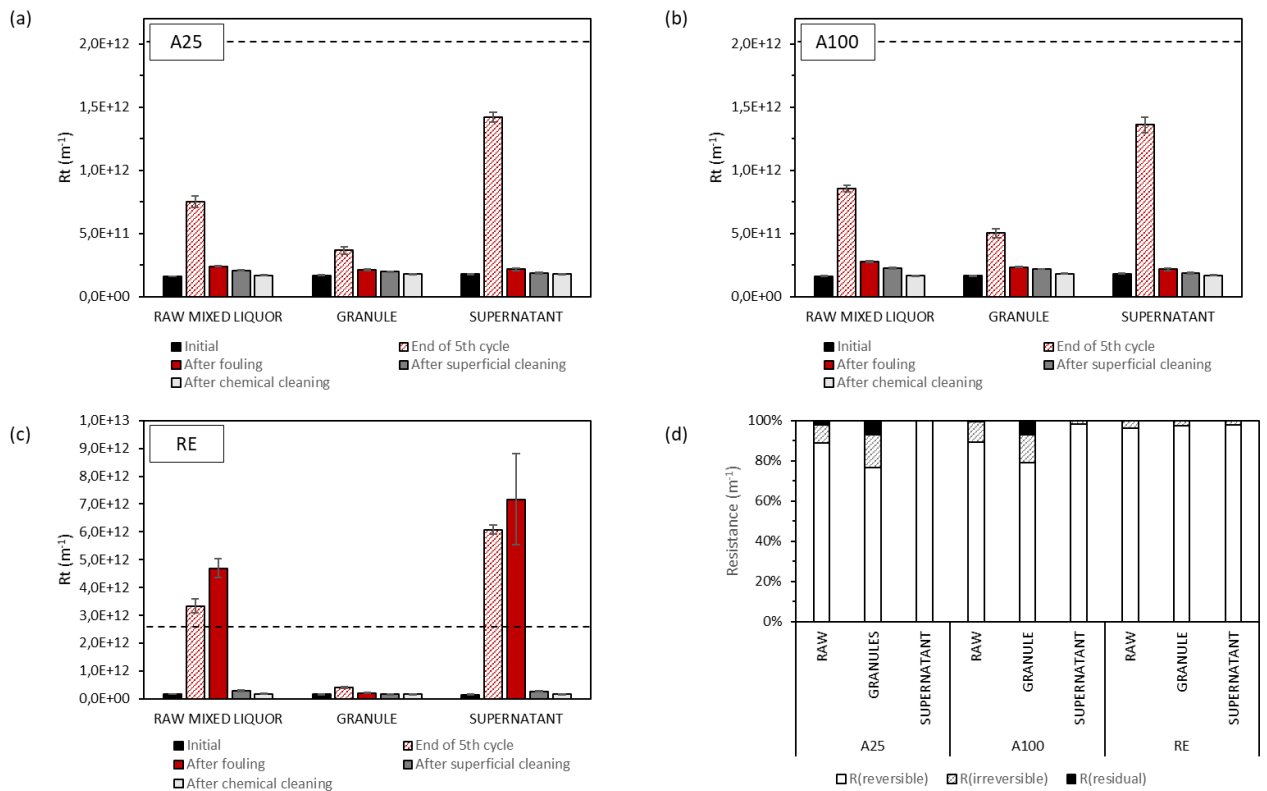
411 Fig. 5d describes the relative reversibility of the fouling deposit for each experiment. In
412 any hydrodynamic condition, the filtration resistance built up during the filtration of the

413 supernatant was predominantly reversible ($\geq 98\%$), meaning that almost all of the fouling
414 was removed by the physical cleaning. Interestingly, for the granule fraction, in both
415 aeration conditions, around 20% of the total resistance remained after superficial cleaning
416 ($R_{\text{irreversible}} + R_{\text{irrecoverable}}$), and 7% of the filtration resistance was not even recovered after
417 chemical cleaning ($R_{\text{irrecoverable}}$). Regarding the raw mixed liquor, about 10% of the fouling
418 resistance remained after physical cleaning. Based on these findings, it could be suggested
419 that different fouling mechanisms were implicated relative to the fraction filtered. During
420 the filtration of the supernatant fraction, the rapid accumulation of micro-particles and
421 fines led to the build-up of a cake layer. Then, under the continuous filtration, the cake
422 layer was compressed, causing the change in cake structure and a shift in particle size
423 distribution to a larger size next to the membrane surface [36]. The cake consolidation
424 allowed for an easier and effective cake removal, since it allows the detachment of large
425 agglomerates and large layer fragments [37]. In contrast, when the supernatant was
426 combined with the granule fraction (i.e. raw mixed liquor), the cake layer was more
427 porous because of larger particle size, which was beneficial for the filtration performance.
428 However, soluble and smallest substances can pass through the loose cake layer and
429 attach to the membrane surface or block the membrane pores [10]. A lower reversibility
430 of small and single particles which interact with the membrane surface has been reported
431 [37] which could explain the measured irreversible and residual resistances.

432 These distributions of the nature of the fouling should be interpreted with caution, because
433 although it describes the relative repartition of the resistances, it does not highlight their
434 effective resistance to the filtration. Hence, even if a part of the fouling caused by granules
435 (i.e. raw and granule fractions) was not removed by the cleaning methods employed, the
436 filtration resistance caused by the persistent foulants was still low compared to the initial
437 filtration resistance ($R_m = 16.5 \pm 1.1 \cdot 10^{10} \text{ m}^{-1}$).

438 In contrast, for all fractions in the RE conditions, the initial resistance was restored almost
439 entirely with the physical cleaning ($\geq 96\%$). In this case, the low hydrodynamic conditions
440 resulted in a barely fixed granular sludge bed, so that the granule fraction was not in the
441 vicinity of the membrane and did not take part of the cake layer formation. Therefore, the
442 membrane fouling that took place during the raw and granule fractions must have been
443 composed of micro-particles and non-settable compounds similar to the supernatant
444 fraction and thus had the same compact structure which induced the same degree of
445 reversibility.

446 Based on these results, a combine fouling mitigation method can be suggested with short
447 intermittent cycles composed of filtration without gas sparging intersected by relaxation
448 and gas sparging periods. In this way, the granules would not be degraded, the fouling
449 deposition would be mostly reversible and the gas sparging energy demand would be
450 lowered. This is in accordance with a previous G-AnMBR study in which, in absence of
451 gas sparging, high fouling resistance was observed, but almost all the accumulated cake
452 was removed by simultaneous use of relaxation and gas sparging [17].



453

454 Fig. 5 – Evolution of the filtration resistance at different operating stages: (i) the initial stage (i.e. $R_t = R_m$),
 455 (ii) the end of the fifth cycle of filtration, (iii) the fouled membrane, (iv) after the superficial cleaning, and
 456 (v) after the chemical cleaning for (a) the 25L/min aeration rate, (b) the 100 L/min aeration rate, (c) the
 457 recirculation, and (d) repartition of the different type of fouling resistance for raw mixed liquor and the two
 458 fractions at different operating conditions.

459

460 3.5 Membrane fouling characteristics

461 Table 1 presents the repartition of the volume of fluorescence obtained through 3DEEM
 462 for rinsing water collected from each superficial cleaning – i.e. the reversible foulant. In
 463 all cases, the largest amount of fluorescence appeared in region I+II, accounting for 68-
 464 85% of the total fluorescence. According to Jacquin et al. (2017), region I+II from the
 465 3DEEM fluorescence is associated with colloidal proteins and, consistent with the present
 466 results, they appeared to be the major foulants in G-AnMBR. It appears that micro-
 467 particles (0.45-10 μm) play a key role in G-AnMBR, as already observed in classical
 468 AnMBR studies [14], and organic foulant compounds are mainly protein-like substances
 469 [38]. The critical role of proteins has already been underlined due to their greater

470 hydrophobicity, which induces a higher adhesion capacity of protein-rich compounds to
471 the polymeric membrane surface [17,39]. The total volume of fluorescence of every
472 fraction in RE conditions was definitely higher than under aeration conditions. It seems
473 that the higher filtration resistance is due to a larger amount of foulants on the membrane
474 surface rather than a different and harsher type of foulant. Moreover, the volume of
475 fluorescence increased in the A100 condition relative to A25 which described a stronger
476 organic matter deposition, certainly linked to the granule disruption and protein release
477 mentioned previously (see Section 3.1).

478 **4. Conclusion**

479 From the present study, the following conclusions can be drawn:

- 480 ▪ Granules ($d_p \geq 0.125$) had a negligible fouling potential with a fouling rate below
481 0.2 mbar.min⁻¹ whatever the hydrodynamic conditions used.
- 482 ▪ The supernatant fraction, composed of fine compounds and flocs ($d_p < 0.125$), was
483 the key driver of membrane fouling in G-AnMBR. Nevertheless, the related
484 membrane fouling was reversible with more than 98% of the fouling resistance
485 recovered by simple water cleaning. Moreover, the compression of the cake layer
486 under the drag forces led to a denser layer, which enables its complete removal.
- 487 ▪ In the raw mixed liquor, where supernatant and granules are mixed, the fouling
488 rate was lower compared to the supernatant fraction. It is suggested that granules
489 diminished the impact of the fines and micro-particles over membrane
490 permeability through mechanical scouring action and the formation of a more
491 porous and loose cake layer structure. Interestingly, around 20% of the total
492 fouling resistance remained after the superficial cleaning, suggesting that the

493 loose cake layer does not prevent small and adherent foulants from entering the
494 membrane pore, causing residual fouling.

495 ■ Based on the 3DEEM analysis, at least 68% of the fluorescent organic matter from
496 the reversible fouling came from the protein-*like* region regardless of the fraction.
497 Hence, colloidal proteins seemed to be the main organic foulant in G-AnMBR.

498 ■ Hydrodynamic conditions were of high importance in mitigating membrane
499 fouling. In tested conditions, gas sparging was more efficient in limiting
500 membrane fouling than recirculation. However, a plateau was reached in gas
501 sparging rate, above which the increase gas flow does not lead to a decrease in
502 fouling rate. Moreover, higher shear stress led to stronger granule disruption,
503 releasing smaller compounds which in turn increased membrane fouling.

504 Based on the results, it is evident that well-shaped and high-strength granules have to be
505 privileged in G-AnMBR. The induced shear forces have to be sufficient to scour the
506 membrane surface whilst not damaging the granular biomass, nor incurring unnecessary
507 energy consumption. The fouling mitigation-energy nexus could lie at an intermittent
508 filtration cycle associated with the threshold sparging rate. Further investigation and
509 technical-economic analysis have to be conducted to define the most favourable filtration
510 cycle which maximises the net energy balance of the G-AnMBR process. In addition,
511 long-term experiments need to be studied to see the potential composition change of the
512 mixed liquor and fractions over time, and its consequences on fouling behaviour.

513 **Acknowledgements**

514 Gaetan Blandin received the support of a fellowship from the “la Caixa” Foundation (ID
515 100010434). The fellowship code is LCF/BQ/PR21/11840009.

516 This work was supported by a grant overseen by the French National Research Agency
517 (ANR) as part of the “JCJC” Programme BâMAN (ANR-18-CE04-0001-01).

518 Table 1 – Repartition of the volume of fluorescence within 3DEEM regions of the superficial cleaning for the three fractions and hydrodynamics conditions studied.

Region	Units	RAW MIXED LIQUOR			GRANULES			SUPERNATANT		
		A25	A100	RE	A25	A100	RE	A25	A100	RE
I+II	$\times 10^9$ (A.U.m ⁻² .L ⁻¹)	2,0 (82.1%)	3,0 (84.8%)	18,3 (81.3%)	1,2 (68.0%)	2,3 (78.4%)	8,3 (78.6%)	1,7 (81.7%)	2,8 (76.0%)	18,0 (85.0%)
IV	$\times 10^9$ (A.U.m ⁻² .L ⁻¹)	0,1 (4.6%)	0,2 (4.4%)	1,5 (6.8%)	0,1 (3.5%)	0,1 (3.6%)	0,4 (3.6%)	0,1 (3.8%)	0,2 (4.1%)	1,3 (6.0%)
III+V	$\times 10^9$ (A.U.m ⁻² .L ⁻¹)	0,3 (13.3%)	0,4 (10.8%)	2,7 (11.8%)	0,5 (28.5%)	0,5 (18.0%)	1,9 (17.8%)	0,3 (14.5%)	0,7 (19.9%)	1,9 (9.0%)
Total	$\times 10^9$ (A.U.m ⁻² .L ⁻¹)	2,4 (100%)	3,6 (100%)	22,6 (100%)	1,8 (100%)	2,9 (100%)	10,6 (100%)	2,0 (100%)	3,7 (100%)	21,1 (100%)

519

520

- 521 [1] M. Maaz, M. Yasin, M. Aslam, G. Kumar, A.E. Atabani, M. Idrees, F. Anjum, F. Jamil,
522 R. Ahmad, A.L. Khan, G. Lesage, M. Heran, J. Kim, Anaerobic membrane bioreactors for
523 wastewater treatment: Novel configurations, fouling control and energy considerations,
524 *Bioresource Technology*. 283 (2019) 358–372.
525 <https://doi.org/10.1016/j.biortech.2019.03.061>.
- 526 [2] L. Sanchez, M. Carrier, J. Cartier, C. Charmette, M. Heran, J.-P. Steyer, G. Lesage,
527 Enhanced organic degradation and biogas production of domestic wastewater at
528 psychrophilic temperature through submerged granular anaerobic membrane bioreactor
529 for energy-positive treatment, *Bioresource Technology*. 353 (2022) 127145.
530 <https://doi.org/10.1016/j.biortech.2022.127145>.
- 531 [3] C. Chen, M. Sun, J. Chang, Z. Liu, X. Zhu, K. Xiao, G. Song, H. Wang, G. Liu, X. Huang,
532 Unravelling temperature-dependent fouling mechanism in a pilot-scale anaerobic
533 membrane bioreactor via statistical modelling, *Journal of Membrane Science*. 644 (2022)
534 120145. <https://doi.org/10.1016/j.memsci.2021.120145>.
- 535 [4] C. Chen, W. Guo, H.H. Ngo, Advances in Granular Growth Anaerobic Membrane
536 Bioreactor (G-AnMBR) for Low Strength Wastewater Treatment, (2016) 7.
- 537 [5] R. Chen, Y. Nie, Y. Hu, R. Miao, T. Utashiro, Q. Li, M. Xu, Y.-Y. Li, Fouling behaviour
538 of soluble microbial products and extracellular polymeric substances in a submerged
539 anaerobic membrane bioreactor treating low-strength wastewater at room temperature,
540 *Journal of Membrane Science*. 531 (2017) 1–9.
541 <https://doi.org/10.1016/j.memsci.2017.02.046>.
- 542 [6] C. Chen, W. Guo, H.H. Ngo, S.W. Chang, D. Duc Nguyen, P. Dan Nguyen, X.T. Bui, Y.
543 Wu, Impact of reactor configurations on the performance of a granular anaerobic
544 membrane bioreactor for municipal wastewater treatment, *International Biodeterioration
& Biodegradation*. 121 (2017) 131–138. <https://doi.org/10.1016/j.ibiod.2017.03.021>.
- 546 [7] O.T. Iorhemen, R.A. Hamza, M.S. Zaghoul, J.H. Tay, Aerobic granular sludge membrane
547 bioreactor (AGMBR): Extracellular polymeric substances (EPS) analysis, *Water
548 Research*. 156 (2019) 305–314. <https://doi.org/10.1016/j.watres.2019.03.020>.
- 549 [8] W. Zhang, W. Liang, Z. Zhang, T. Hao, Aerobic granular sludge (AGS) scouring to
550 mitigate membrane fouling: Performance, hydrodynamic mechanism and contribution
551 quantification model, *Water Research*. 188 (2021) 116518.
552 <https://doi.org/10.1016/j.watres.2020.116518>.
- 553 [9] O.T. Iorhemen, R.A. Hamza, J.H. Tay, Membrane fouling control in membrane
554 bioreactors (MBRs) using granular materials, *Bioresource Technology*. 240 (2017) 9–24.
555 <https://doi.org/10.1016/j.biortech.2017.03.005>.
- 556 [10] B. Zhang, D. Huang, Y. Shen, W. Yin, X. Gao, B. Zhang, W. Shi, Treatment of municipal
557 wastewater with aerobic granular sludge membrane bioreactor (AGMBR): Performance
558 and membrane fouling, *Journal of Cleaner Production*. 273 (2020) 123124.
559 <https://doi.org/10.1016/j.jclepro.2020.123124>.
- 560 [11] I. Martin-Garcia, M. Mocosch, A. Soares, M. Pidou, B. Jefferson, Impact on reactor
561 configuration on the performance of anaerobic MBRs: Treatment of settled sewage in
562 temperate climates, *Water Research*. 47 (2013) 4853–4860.
563 <https://doi.org/10.1016/j.watres.2013.05.008>.
- 564 [12] W. Zhang, F. Jiang, Membrane fouling in aerobic granular sludge (AGS)-membrane
565 bioreactor (MBR): Effect of AGS size, *Water Research*. 157 (2019) 445–453.
566 <https://doi.org/10.1016/j.watres.2018.07.069>.
- 567 [13] C. Xu, Z. Li, J. Wang, Z. Zhou, Exposure to stressful conditions alters the properties and
568 fouling behavior of suspended microparticles in anaerobic processes, *Journal of
569 Environmental Chemical Engineering*. 9 (2021) 106782.
570 <https://doi.org/10.1016/j.jece.2021.106782.a>

- 571 [14] Y. Yao, Z. Zhou, D.C. Stuckey, F. Meng, Micro-particles—A Neglected but Critical
572 Cause of Different Membrane Fouling between Aerobic and Anaerobic Membrane
573 Bioreactors, *ACS Sustainable Chem. Eng.* 8 (2020) 16680–16690.
574 <https://doi.org/10.1021/acssuschemeng.0c06502>.
- 575 [15] K.M. Wang, N.M. Garcia, A. Soares, B. Jefferson, E.J. McAdam, Comparison of fouling
576 between aerobic and anaerobic MBR treating municipal wastewater, *H2Open Journal*. 1
577 (2018) 131–159. <https://doi.org/10.2166/h2oj.2018.109>.
- 578 [16] S. Vinardell, L. Sanchez, S. Astals, J. Mata-Alvarez, J. Dosta, M. Heran, G. Lesage,
579 Impact of permeate flux and gas sparging rate on membrane performance and process
580 economics of granular anaerobic membrane bioreactors, *Science of The Total
581 Environment*. 825 (2022) 153907. <https://doi.org/10.1016/j.scitotenv.2022.153907>.
- 582 [17] K.M. Wang, D. Cingolani, A.L. Eusebi, A. Soares, B. Jefferson, E.J. McAdam,
583 Identification of gas sparging regimes for granular anaerobic membrane bioreactor to
584 enable energy neutral municipal wastewater treatment, *Journal of Membrane Science*. 555
585 (2018) 125–133. <https://doi.org/10.1016/j.memsci.2018.03.032>.
- 586 [18] A. Alphenaar, Anaerobic granular sludge: characterization, and factors affecting its
587 functioning, Wageningen Agricultural University, 1994. <https://edepot.wur.nl/202099>.
- 588 [19] J. O'Reilly, C. Lee, F. Chinalia, G. Collins, T. Mahony, V. O'Flaherty, Microbial
589 community dynamics associated with biomass granulation in low-temperature (15°C)
590 anaerobic wastewater treatment bioreactors, *Bioresource Technology*. 101 (2010) 6336–
591 6344. <https://doi.org/10.1016/j.biortech.2010.03.049>.
- 592 [20] C. Chen, W.S. Guo, H.H. Ngo, Y. Liu, B. Du, Q. Wei, D. Wei, D.D. Nguyen, S.W. Chang,
593 Evaluation of a sponge assisted-granular anaerobic membrane bioreactor (SG-AnMBR)
594 for municipal wastewater treatment, *Renewable Energy*. 111 (2017) 620–627.
595 <https://doi.org/10.1016/j.renene.2017.04.055>.
- 596 [21] P. Le Clech, B. Jefferson, I.S. Chang, S.J. Judd, Critical flux determination by the flux-
597 step method in a submerged membrane bioreactor, *Journal of Membrane Science*. 227
598 (2003) 81–93. <https://doi.org/10.1016/j.memsci.2003.07.021>.
- 599 [22] APHA, AWWA, WEF, eds., *Standard methods: for the examination of water and
600 wastewater*, 20. ed, American Public Health Association, Washington, DC, 1998.
- 601 [23] R. Zepp, W. Sheldon, M.A. Moran, Dissolved organic fluorophores in southeastern US
602 coastal waters: Correction method for eliminating Rayleigh and Raman scattering peaks
603 in excitation-emission matrices, *Marine Chemistry*. 89 (2004) 15–36.
604 <https://doi.org/10.1016/j.marchem.2004.02.006>.
- 605 [24] C. Jacquin, G. Lesage, J. Traber, W. Pronk, M. Heran, Three-dimensional excitation and
606 emission matrix fluorescence (3DEEM) for quick and pseudo-quantitative determination
607 of protein- and humic-like substances in full-scale membrane bioreactor (MBR), *Water
608 Res.* 118 (2017) 82–92. <https://doi.org/10.1016/j.watres.2017.04.009>.
- 609 [25] M. Dubois, K. Gilles, J.K. Hamilton, P.A. Rebers, F. Smith, A Colorimetric Method for
610 the Determination of Sugars, *Nature*. 168 (1951) 167–167.
611 <https://doi.org/10.1038/168167a0>.
- 612 [26] OliverH. Lowry, NiraJ. Rosebrough, A.L. Farr, RoseJ. Randall, Protein measurement with
613 the Folin phenol reagent, *Journal of Biological Chemistry*. 193 (1951) 265–275.
614 [https://doi.org/10.1016/S0021-9258\(19\)52451-6](https://doi.org/10.1016/S0021-9258(19)52451-6).
- 615 [27] J. Wu, Z.Y. Lu, J.C. Hu, L. Feng, J.D. Huang, X.S. Gu, Disruption of granules by
616 hydrodynamic force in internal circulation anaerobic reactor, *Water Sci Technol*. 54
617 (2006) 9–16. <https://doi.org/10.2166/wst.2006.868>.
- 618 [28] Z. Zhou, Y. Tao, S. Zhang, Y. Xiao, F. Meng, D.C. Stuckey, Size-dependent microbial
619 diversity of sub-visible particles in a submerged anaerobic membrane bioreactor

- 620 (SAnMBR): Implications for membrane fouling, *Water Research*. 159 (2019) 20–29.
621 <https://doi.org/10.1016/j.watres.2019.04.050>.
- 622 [29] D. Jeison, J.B. van Lier, Cake layer formation in anaerobic submerged membrane
623 bioreactors (AnSMBR) for wastewater treatment, *Journal of Membrane Science*. 284
624 (2006) 227–236. <https://doi.org/10.1016/j.memsci.2006.07.035>.
- 625 [30] A. Massé, M. Spérandio, C. Cabassud, Comparison of sludge characteristics and
626 performance of a submerged membrane bioreactor and an activated sludge process at high
627 solids retention time, *Water Research*. 40 (2006) 2405–2415.
628 <https://doi.org/10.1016/j.watres.2006.04.015>.
- 629 [31] L. Böhm, A. Drews, H. Prieske, P.R. Bérubé, M. Kraume, The importance of fluid
630 dynamics for MBR fouling mitigation, *Bioresource Technology*. 122 (2012) 50–61.
631 <https://doi.org/10.1016/j.biortech.2012.05.069>.
- 632 [32] E. Nguyen Cong Duc, L. Fournier, C. Levecq, B. Lesjean, P. Grelier, A. Tazi-Pain, Local
633 hydrodynamic investigation of the aeration in a submerged hollow fibre membranes
634 cassette, *Journal of Membrane Science*. 321 (2008) 264–271.
635 <https://doi.org/10.1016/j.memsci.2008.05.001>.
- 636 [33] S. Chellam, M.R. Wiesner, Particle Back-Transport and Permeate Flux Behavior in
637 Crossflow Membrane Filters, *Environ. Sci. Technol.* 31 (1997) 819–824.
638 <https://doi.org/10.1021/es9605228>.
- 639 [34] E. Tardieu, A. Grasmick, V. Geaugey, J. Manem, Hydrodynamic control of bioparticle
640 deposition in a MBR applied to wastewater treatment, *Journal of Membrane Science*. 147
641 (1998) 1–12. [https://doi.org/10.1016/S0376-7388\(98\)00091-X](https://doi.org/10.1016/S0376-7388(98)00091-X).
- 642 [35] H. Lin, W. Peng, M. Zhang, J. Chen, H. Hong, Y. Zhang, A review on anaerobic
643 membrane bioreactors: Applications, membrane fouling and future perspectives,
644 *Desalination*. 314 (2013) 169–188. <https://doi.org/10.1016/j.desal.2013.01.019>.
- 645 [36] W.J. Gao, H.J. Lin, K.T. Leung, H. Schraft, B.Q. Liao, Structure of cake layer in a
646 submerged anaerobic membrane bioreactor, *Journal of Membrane Science*. 374 (2011)
647 110–120. <https://doi.org/10.1016/j.memsci.2011.03.019>.
- 648 [37] J. Altmann, S. Ripperger, Particle deposition and layer formation at the crossflow
649 microfiltration, *Journal of Membrane Science*. 124 (1997) 119–128.
650 [https://doi.org/10.1016/S0376-7388\(96\)00235-9](https://doi.org/10.1016/S0376-7388(96)00235-9).
- 651 [38] H. Yang, Z. Li, Y. Chen, Z. Zhou, Role of microparticles in membrane fouling from
652 acidogenesis to methanogenesis phases in an anaerobic baffled reactor, *Science of The
653 Total Environment*. 806 (2022) 150663. <https://doi.org/10.1016/j.scitotenv.2021.150663>.
- 654 [39] Z. Yang, Q.N. Tran, X. Jin, Ultrafiltration of aerobic granular sludge bioreactor effluent:
655 Fouling potentials and properties, *Journal of Water Process Engineering*. 47 (2022)
656 102805. <https://doi.org/10.1016/j.jwpe.2022.102805>.
- 657